Scaling the discrete Fourier transform gate in the quantum frequency processor

Hsuan-Hao Lu,^{1,*} Navin B. Lingaraju,¹ Daniel E. Leaird,¹ Andrew M. Weiner,¹ and Joseph M. Lukens^{2,†}

¹ School of Electrical and Computer Engineering and Purdue Quantum Science and Engineering Institute, Purdue University, West Lafayette, Indiana 47907, USA
² Quantum Information Science Group, Oak Ridge National Laboratory, Oak Ridge, Tennessee 37831, USA
*peach811215@gmail.com
†lukensjm@ornl.gov

Abstract: We show that the d-dimensional discrete Fourier transform can be implemented by adding RF harmonics to the applied modulation in a quantum frequency processor. Implementing the d=3 case experimentally, we quantify entanglement and perform full quantum state tomography. © 2021 The Author(s)

Mutually unbiased bases (MUBs) enable important applications in quantum information processing, including efficient quantum tomography [1], quantum key distribution [2], and entanglement quantification [3, 4]. Two representative MUBs are the computational and Fourier bases, defined for $m \in \{0,...,d-1\}$ as $|m\rangle$ and $|f_m\rangle = \frac{1}{\sqrt{d}}\sum_{n=0}^{d-1}e^{-2\pi i mn/d}|n\rangle$, respectively. The Fourier basis is so-named because it can be measured by applying the discrete Fourier transform (DFT) matrix with elements $(F_d)_{mn} = \frac{1}{\sqrt{d}}e^{2\pi i mn/d}$ followed by computational-basis detection. In the context of frequency-bin qudits, the DFT has been synthesized up to d=3 on a quantum frequency processor (QFP) [5]. In this work, we simulate designs for higher-dimensional DFTs, finding a remarkable scaling rule, valid at least up to the maximum of d=10 considered: a fixed three-element QFP can realize the d-dimensional DFT by driving each electro-optic modulator with d-1 RF tones. As an example application, we experimentally implement parallel d=3 DFT gates on frequency-bin-entangled photons, using the measurements to estimate the complete density matrix. Overall, our results offer a clear path forward for DFT gate synthesis in frequency-bin quantum information, valuable for quantifying and leveraging entanglement.

In order to interfere discrete frequency bins spaced at $\Delta\omega$, we start with electro-optic phase modulators (EOMs) driven by waveforms periodic at $\Delta \omega$. As observed in Ref. [5], a lone single-pass EOM cannot mix d frequency bins equally without at least $\frac{d-1}{2d-1}$ of the input energy scattering into modes outside of the d-dimensional subspace. However, by cascading multiple EOMs separated by pulse shapers—the QFP—this scattering can be compensated and high-probability, high-fidelity mixing is possible. In the first demonstration of the d=2 and d=3 DFTs on an EOM/pulse-shaper/EOM QFP, the d=2 case utilized single-frequency sinewave modulation, while the d=3solution required modulation containing both the first and second harmonic. To see if this "add-RF-harmonic" rule represents a trend for DFT gates, we perform additional design simulations for a three-element QFP. The matrix fidelity \mathcal{F}_W and success probability \mathcal{P}_W [6] results for d-dimensional DFT gates follow in Fig. 1(a), where in each case we consider d-1 tones in the optimization procedure. For all dimensions, solutions with $\mathcal{F}_W > 0.9997$ and $\mathcal{P}_W > 0.965$ are possible with these resources. Significantly, the number of elements required is constant in d, rather than linear in d as expected for either arbitrary gates [6] or the DFT when only single-tone modulation is considered [7]. Nevertheless, the effective number of modes utilized does increase with d, as expressed by the vertical lines in Fig. 1(a), which mark where the third significant digit of the cost $\mathcal{P}_W \log_{10}(1-\mathcal{F}_W)$ has converged to its limiting value, suggesting a tradeoff between circuit depth and optical bandwidth. From a practical side, accessing additional bandwidth is frequently preferred to adding components—both in terms of cost and loss budget—so that this fixed-depth DFT design procedure appears quite useful, particularly toward on chip

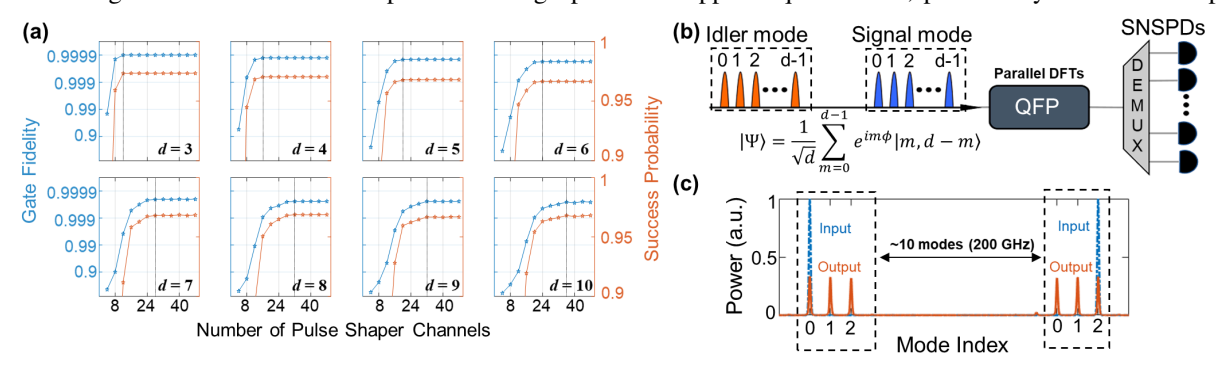
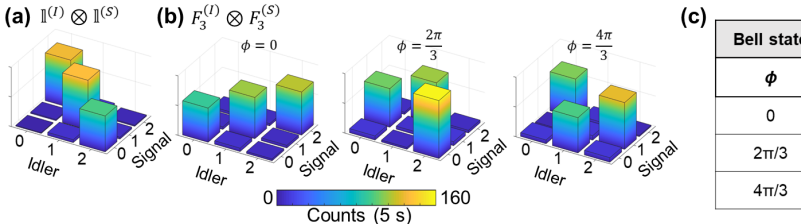


Fig. 1. (a) DFT solutions. (b) Parallel DFT experiment. (c) Modes defined for d = 3 implementation.



Bell state	Entropy	QST	
φ	min E _D	${\cal F}_{ ho}$	$\boldsymbol{E}_{\scriptscriptstyle\mathcal{N}}$
0	0.41 ± 0.09	0.84 ± 0.02	1.40 ± 0.03
2π/3	0.41 ± 0.09	0.84 ± 0.02	1.40 ± 0.03
4π/3	0.36 ± 0.09	0.83 ± 0.02	1.40 ± 0.04

Fig. 2. Coincidences for (a) $\mathbb{1}^{(I)} \otimes \mathbb{1}^{(S)}$ and (b) $F_3^{(I)} \otimes F_3^{(S)}$ operations. (c) Characterization results.

integration where tighter mode spacings could make high-order RF harmonics much more readily attainable.

As an application of the DFT for state characterization, we experimentally implement the d=3 solution and apply it to a biphoton frequency comb, prepared by spontaneous parametric downconversion followed by a pulse shaper to carve 20 GHz-spaced, ~ 10 GHz-wide bins. Figure 1(b) provides a conceptual illustration of our experimental design for d=3. While previously demonstrated on single-photon states [5], this is the first example of parallel implementation on an entangled qutrit pair. The bin spacing $\Delta\omega/2\pi=20$ GHz is chosen for line-by-line shaping with our QFP pulse shaper, so that RF tones at 20 and 40 GHz are required at each of the QFP's two EOMs. Figure 1(c) shows an example mode transformation spectrum for the parallel DFT operation.

A logical basis measurement of our 3×3 biphoton frequency comb (EOMs off) appears in Fig. 2(a). Using the front-end pulse shaper to produce biphoton states ideally of the form $|\phi\rangle \propto |02\rangle_{IS} + e^{i\phi} |11\rangle_{IS} + e^{2i\phi} |20\rangle_{IS}$, the measured output coincidences for $\phi \in \{0, 2\pi/3, 4\pi/3\}$ after parallel DFTs follow in Fig. 2(b): as expected, the results are strongly correlated, with each setting of ϕ determining which three pairs of frequency bins are populated. Despite the small number of measurements considered, the observed correlations are sufficient to make meaningful inferences of the underlying states. Since the prepared states differ only in phase, we can take the logical basis results as applying to any of the three ϕ cases, giving us two sets of nine-outcome measurements for each ϕ value, $\mathbb{I}^{(I)} \otimes \mathbb{I}^{(S)}$ and $F_3^{(I)} \otimes F_3^{(S)}$. One useful metric for a bipartite state is the distillable entanglement E_D : the optimal rate of Bell pair production given many state copies, allowing for local operations and classical communication. While extremely difficult to determine directly, bounds can be obtained from computable quantities. For example, a lower bound can be set from conditional entropies [3], namely: $E_D \geq \log_2 3 - \mathcal{H}(\mathbb{I}^{(I)} |\mathbb{I}^{(S)}) - \mathcal{H}(F_3^{(I)} |F_3^{(S)})$. With classical Bayesian inference (no quantum mechanical constraints), we find the min E_D values in Fig. 2(c).

In addition, E_D can be upper bounded by the log-negativity $E_{\mathscr{N}}$ [8]; however, a full density matrix is required for such a computation. Utilizing Bayesian tomographic methods [9], which return uncertainties commensurate with the data gathered, we can indeed estimate the full quantum state with these results. The Bayesian fidelities for each state ($\mathscr{F}_p = \langle \phi | \rho | \phi \rangle$) are shown in Fig. 2(c). Since the outcomes are so strongly correlated, the inferred states have small uncertainty, even with just two measurements. Computing the log-negativity $E_{\mathscr{N}}$ (the upper bound of E_D [8]), we obtain a complete interval for E_D of approximately $E_D \in [0.4, 1.4]$ ebits for the states considered. This range is quite wide, and we suspect that the much higher values for $E_{\mathscr{N}}$ result from its application of quantum state constraints, in contrast to the entropic approach which treats the measurement results as raw probabilities. It would be interesting to explore how this range may narrow with higher-fidelity results, which are limited here primarily by the resolution of the state preparation and measurement pulse shapers.

We thank AdvR for loaning a PPLN ridge waveguide. This work was performed in part at Oak Ridge National Laboratory, operated by UT-Battelle for the U.S. Department of Energy under contract no. DE-AC05-00OR22725. Funding was provided by the STTR Agreement under AFRL Prime Order No. FA8750-20-P-1705; the U.S. Department of Energy, Office of Advanced Scientific Computing Research, Early Career Research Program; and the National Science Foundation (1839191-ECCS, 1747426-DMR).

References

- 1. W. K. Wootters and B. D. Fields, Ann. Phys. 191, 363 (1989).
- 2. L. Sheridan and V. Scarani, Phys. Rev. A 82, 030301 (2010).
- 3. P. J. Coles, M. Berta, M. Tomamichel, and S. Wehner, Rev. Mod. Phys. 89, 015002 (2017).
- 4. J. Bavaresco, N. H. Valencia, C. Klöckl, M. Pivoluska, P. Erker, N. Friis, M. Malik, and M. Huber, Nat. Phys. 14, 1032 (2018).
- 5. H.-H. Lu, J. M. Lukens, N. A. Peters, O. D. Odele, D. E. Leaird, A. M. Weiner, and P. Lougovski, Phys. Rev. Lett. **120**, 030502 (2018).
- 6. J. M. Lukens and P. Lougovski, Optica 4, 8 (2017).
- 7. J. M. Lukens, H.-H. Lu, B. Qi, P. Lougovski, A. M. Weiner, and B. P. Williams, J. Lightwave Technol. 38, 1678 (2020).
- 8. G. Vidal and R. F. Werner, Phys. Rev. A 65, 032314 (2002).
- 9. J. M. Lukens, K. J. H. Law, A. Jasra, and P. Lougovski, New J. Phys. 22, 063038 (2020).